



Photochemical grid model implementation and application of VOC, NO_x, and O₃ source apportionment

R. H. F. Kwok¹, K. R. Baker¹, S. L. Napelenok¹, and G. S. Tonnesen²

¹United States Environmental Protection Agency, 109 T.W. Alexander Drive, Research Triangle Park, NC 27711, USA

²United States Environmental Protection Agency, Region 8, 1595 Wynkoop Street, Denver, CO 80202-1129, USA

Correspondence to: S. L. Napelenok (napelenok.sergey@epa.gov)

Received: 15 July 2014 – Published in Geosci. Model Dev. Discuss.: 3 September 2014

Revised: 3 December 2014 – Accepted: 16 December 2014 – Published: 29 January 2015

Abstract. For the purposes of developing optimal emissions control strategies, efficient approaches are needed to identify the major sources or groups of sources that contribute to elevated ozone (O₃) concentrations. Source-based apportionment techniques implemented in photochemical grid models track sources through the physical and chemical processes important to the formation and transport of air pollutants. Photochemical model source apportionment has been used to track source impacts of specific sources, groups of sources (sectors), sources in specific geographic areas, and stratospheric and lateral boundary inflow on O₃. The implementation and application of a source apportionment technique for O₃ and its precursors, nitrogen oxides (NO_x) and volatile organic compounds (VOCs), for the Community Multiscale Air Quality (CMAQ) model are described here. The Integrated Source Apportionment Method (ISAM) O₃ approach is a hybrid of source apportionment and source sensitivity in that O₃ production is attributed to precursor sources based on O₃ formation regime (e.g., for a NO_x-sensitive regime, O₃ is apportioned to participating NO_x emissions). This implementation is illustrated by tracking multiple emissions source sectors and lateral boundary inflow. NO_x, VOC, and O₃ attribution to tracked sectors in the application are consistent with spatial and temporal patterns of precursor emissions. The O₃ ISAM implementation is further evaluated through comparisons of apportioned ambient concentrations and deposition amounts with those derived from brute force zero-out scenarios, with correlation coefficients ranging between 0.58 and 0.99 depending on specific combination of target species and tracked precursor emissions. Low correlation coefficients occur for chemical regimes that have strong nonlinearity in O₃ sensitivity, which demonstrates different func-

tionality between source apportionment and zero-out approaches, where appropriate use depends on whether source attribution or source sensitivity is desired.

1 Introduction

Regulatory programs have been in place in the United States for more than 50 years to reduce ambient exposure to ozone (O₃) which has harmful effects on human health and vegetation (Bell et al., 2004; U.S. Environmental Protection Agency (EPA), 2009; National Research Council, 1991). Nevertheless, many areas continue to exceed the national ambient air quality standard (NAAQS) for ozone, and uncertainty remains in both the local and distant sources that contribute to exceedances of the NAAQS. The EPA has set a NAAQS for O₃, where compliance with the NAAQS is determined as the 3-year average of the fourth highest daily maximum 8 h average O₃. In areas that violate the NAAQS, the states and tribes must develop plans to attain the NAAQS by reducing emissions of O₃ precursors, including volatile organic compounds (VOCs) and nitrogen oxides (NO_x). Additionally, Sect. 110(a)(2)(D) of the Clean Air Act requires states, in part, to eliminate significant contribution to nonattainment of the NAAQS in other states. To develop effective O₃ attainment plans, it is important to understand the sources of ozone that contribute to violations of the NAAQS. Sources of O₃ can include local sources, long-range transport (L. Zhang et al., 2008; Zhang et al., 2009; Lin et al., 2012), stratospheric intrusion (Langford et al., 2009), and photochemical production of O₃ (PO₃) from a wide variety of biogenic and anthropogenic VOC and NO_x precursors

(Haagen-Smit and Fox, 1954; Lefohn et al., 2014). For air quality managers who are tasked with developing the most expeditious and cost effective emissions control strategies, it is useful to have methods to identify the relative importance of sources that contribute to high O₃ concentrations, and to predict how O₃ will respond to reductions in VOC and NO_x precursor emissions. Specifically, it is useful to quantify the relative amount of O₃ originating from specific VOC and NO_x emissions sources (or groups of sources, such as an emissions sector), as well as to distinguish locally produced O₃ from O₃ that is transported from upwind sources. Source sensitivity and apportionment approaches have been used to estimate intercontinental ozone contribution (Anenberg et al., 2010; Sudo and Akimoto, 2007; L. Zhang et al., 2009), and contribution from specific geographic areas (Tong and Mauzerall, 2008), emissions sectors (Fann et al., 2013; X. Wang et al., 2009; Ying and Krishnan, 2010), and single sources (Bergin et al., 2008). The Integrated Source Apportionment Method (ISAM) for PM_{2.5} was previously implemented in the Community Multiscale Air Quality (CMAQ) model (Kwok et al., 2013). Here, the ISAM implementation is extended to analysis of O₃ source apportionment. This implementation is compared directly with source sensitivity apportionment approaches to provide confidence in the implementation.

2 Review of ozone source apportionment methods

Various methods have been applied to characterize and quantify the relationship between emission sources and ozone concentrations including statistical methods, model sensitivity simulations, and model source apportionment approaches (Cohan and Napelenok, 2011). Statistical approaches using ambient data trends (Porter et al., 2001) or ambient data paired with emissions source characteristics (Kenski et al., 1995; Scheff and Wadden, 1993) have been used in the past as methods for ozone source attribution. Receptor-based approaches such as the chemical mass balance (CMB) or positive matrix factorization (PMF) receptor models provide information about source attribution to ozone precursors, but not directly to ozone (Buzcu and Fraser, 2006; Chung et al., 1996; Kim et al., 2005; Scheff et al., 1996; Tong et al., 2005). Statistical correlation analyses of the regional ozone pattern and time-lagged correlation analyses have also been used to analyze transport effects (Guinnup and Collom, 1997; Husar and Renard, 1997). These studies concluded that transport of O₃ and precursors could occur over the distance of 300–600 km, but did not clearly differentiate the specific origins of transported ozone or the confounding effects of meteorological factors (Guinnup and Collom, 1997).

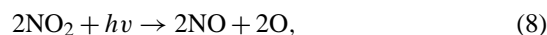
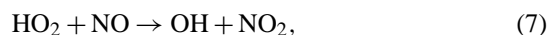
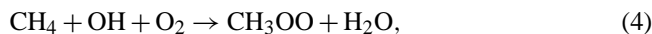
Air quality model sensitivity simulations have been widely used to predict how O₃ responds to changes in specific sources of emissions of VOCs and NO_x (Russell and Dennis, 2000). Source sensitivity approaches include photochemical

model “brute force” simulations, in which a single emission source is reduced or removed, and also model extensions that in a single simulation track multiple emissions sensitivities forward (decoupled direct method, DDM) (Dunker et al., 2002) or backward (adjoint) (Mesbah et al., 2012). Model sensitivity approaches have limitations when used for total source culpability, however, because of the nonlinear dependence of O₃ on concentrations of VOCs and NO_x. This is especially problematic for evaluating contributions of NO_x because O₃ can have negative sensitivity to NO_x in situations where the ratio of VOCs to NO_x is low. Therefore, summing the O₃ change in response to sensitivity simulations for multiple emissions sources can result in difficulty interpreting the cumulative effect of those emissions on O₃.

In source apportionment approaches, the objective is to identify the amount of O₃ produced by particular emissions sources rather than determining the sensitivity of O₃ to those sources. This distinction is important in cases where O₃ has a nonlinear sensitivity or negative sensitivity to changes in emissions. Source apportionment methods also have the benefit of estimating contributions from many different VOC and NO_x source categories in a single model simulation. To describe the different approaches used in source apportionment methods, it is helpful to review the chemistry of O₃ formation. In the troposphere, O₃, nitrogen oxide (NO) and nitrogen dioxide (NO₂) react rapidly in a photo-stationary state (PSS) null cycle, shown in Reactions (1–3), which has no net effect on ambient O₃ concentrations:



Photochemical formation of O₃ (PO₃) in the troposphere occurs almost exclusively by the oxidation of VOCs (Finlayson-Pitts and Pitts, 1986), as illustrated in Reactions (4)–(7) using methane (CH₄) reactions. While O₃ is not formed directly, Reactions (5) and (7) provide alternate pathways to convert NO to NO₂ without the loss of O₃ in Reaction (1), thereby allowing O₃ to accumulate as shown in the net reaction of (1) to (9):



Net reaction:



Because multiple families of precursors participate in the photochemical formation of O₃ (PO₃), including NO_x, VOCs

and free radicals ($\text{HO}_x = \text{OH} + \text{HO}_2 + \text{RO}_2$), the developer of a mass apportionment method for sources of PO_3 must determine which precursor is of primary interest for source apportionment. For example, PO_3 can be apportioned only on the basis of the NO_x emissions sources, or VOC emissions sources, or sources of HO_x that contribute to PO_3 in Reactions (4–7). Alternatively, a hybrid approach can be used that combines attribution to multiple families of precursors, in which PO_3 is attributed to either VOC or NO_x sources depending on whether PO_3 occurs under VOC- or NO_x -sensitive conditions.

Ozone source apportionment approaches have been implemented in a number of regional air quality models including the Comprehensive Air-quality Model with Extensions (CAMx) (ENVIRON, 2013), the Model for Ozone and Related chemical Tracers (MOZART-4) (Emmons et al., 2012), the Weather Research and Forecasting with Chemistry (WRF-Chem) model (Pfister et al., 2013), and the Community Multiscale Air Quality (CMAQ) model version 4.6 (Arunachalam, 2010; Ying and Krishnan, 2010).

Each of the above approaches augments the model by adopting a system of tracer species to track the sources of ozone and its precursor species for selected groupings of emissions categories and geographical regions. It is useful to define the “bulk” concentration as the model simulated concentration of a given species in the unaugmented model, where the bulk concentration should be identical to the sum of the tracers, e.g.,

$$C_{\text{bulk},\text{O}_3}^{i,j,k} = \sum_{n=1}^N C_{\text{O}_3n}^{i,j,k}, \quad (10)$$

$$C_{\text{bulk},\text{VOC}}^{i,j,k} = \sum_{n=1}^N C_{\text{VOC}_n}^{i,j,k}, \quad (11)$$

$$C_{\text{bulk},\text{NO}_x}^{i,j,k} = \sum_{n=1}^N C_{\text{NO}_xn}^{i,j,k}, \quad (12)$$

where N represents the number of tracers needed to represent all sources that contribute to the bulk species concentration, and i, j, k represent cells within the 3-dimensional grid. While each of the models identified above is augmented with a set of tracers, there are significant differences used in source apportionment for these models that are summarized below.

The CAMx Ozone Source Apportionment Technology (OSAT) includes tracers for O_3 and for the families of reactive NO_x and VOC species. The ratio of production of hydrogen peroxide to nitric acid ($\text{PH}_2\text{O}_2 / \text{PHNO}_3$) is used to determine if PO_3 occurs in either a NO_x - or VOC-sensitive chemical regime ($\text{PH}_2\text{O}_2 / \text{PHNO}_3$ above or below 0.35, respectively; Sillman 1995). If PO_3 occurs in a NO_x -sensitive regime, the NO_x tracers are used to attribute PO_3 proportionally to the emissions sources that contributed to the NO_x concentration. Alternatively, if PO_3 occurs in a VOC-

sensitive regime, the VOC tracers are used to attribute PO_3 to the emissions sources that contributed to the VOC concentration. CAMx OSAT does not include tracers for individual VOC species. Instead, to reduce computational cost, the source attribution is based on a VOC family tracer, defined as the reactivity weighted sum of the emissions of individual VOC species for each source category. The VOC tracer decays based on an estimate of its reactivity with OH, and the VOC tracer’s contribution to PO_3 is estimated based on its maximum incremental reactivity (MIR) (Carter, 1994). The adjustment using MIR also accounts for increased PO_3 from highly reactive VOCs, such as aldehydes and aromatics, which can also act as sources of OH radicals (Jeffries and Tonnesen, 1994). O_3 production and destruction reactions operate simultaneously within the chemical mechanism, so the net change in ozone during a chemistry solver time step in the model simulation is the sum of production and loss:

$$\Delta\text{O}_3 = \text{PO}_3 + \text{DO}_3, \quad (13)$$

where $\text{DO}_3 \leq 0$ indicates chemical destruction of O_3 . In CAMx OSAT, PO_3 is estimated as the net change in O_3 during the chemistry time step combined with amount of chemical destruction of O_3 :

$$\text{PO}_3 = \Delta\text{O}_3 - \text{DO}_3. \quad (14)$$

PO_3 is used to update the O_3 tracers attributed to VOC and NO_x emissions sources, and in a separate step the O_3 tracers are reduced by DO_3 . CAMx OSAT does not consider the reaction of O_3 with NO as chemical destruction, because this reaction occurs as part of the PSS null cycle in Reactions (1–3) that neither produces nor destroys O_3 . Finally, it should be noted that CAMx OSAT adopts tracers that are updated at each chemistry time step based on chemical reaction rates, but these tracers are not added to the chemical mechanism and therefore do not increase the computational cost of the numerical chemistry algorithm.

In contrast to CAMx OSAT, the MOZART and WRF-Chem models both adopt a source apportionment method that augments the chemical mechanism with additional species and duplicative reactions that acts as tracer of emissions sources of NO_x . O_3 tracers are updated based only on their attribution to NO_x . These adaptations are primarily appropriate at the global scale, where PO_3 is primarily NO_x -limited, and tagging NO_x was an appropriate choice for that purpose (Emmons et al., 2012). However, the MOZART and WRF-Chem source apportionment approach treats Reaction (1) as chemical destruction of O_3 , so that when a stratospheric or boundary condition (BC) O_3 molecule reacts with an anthropogenic NO molecule via Reaction (1), the O_3 that is subsequently formed in Reactions (2) and (3) is considered anthropogenic. Because the PSS null cycle does not result in any net PO_3 , the approach used in MOZART and WRF-Chem could artificially convert tracers of stratospheric and BC O_3 to anthropogenic O_3 and overestimate the contribution of anthropogenic NO_x to O_3 .

Ying and Krishnan (2010) implemented a source apportionment algorithm in CMAQ that relies on a set of additional species and duplicative reactions that act as tracers of O₃ produced from individual VOC species. In this case, the model developers were primarily concerned with O₃ attribution to anthropogenic and biogenic VOCs in the urban ozone nonattainment area, and therefore tracers were only evaluated for VOC species. The algorithm used the NO₂ production rates in Reactions (5) and (7) to represent PO₃, so this method has the benefit of representing total photochemical production of odd oxygen (O_x) which is defined as the sum of O₃, NO₂ and other species that act as a reservoir of atomic oxygen. However, this approach does not consider the effects that highly reactive VOC species have on production of new radical species, which also affects the PO₃. Therefore, this approach may underestimate the contribution of high reactivity VOCs and overestimate the contribution of low reactivity VOCs to PO₃. Additionally, because of the large number of additional tracer species and reactions included in the photochemical mechanism, and the resulting increased computational cost, only one VOC emissions source category could be included in each simulation.

Ozone source attribution analysis can also be performed using the process analysis and integrated reaction rate outputs in the CMAQ and CAMx models. Each model has the option to store hourly mass throughput for each reaction in the chemical mechanism, and postprocessing can be performed to attribute ozone to VOC and NO_x precursors when these processes are coupled with tools such as Lagrangian trajectory models to track source specific transport (Henderson et al., 2011). While these approaches are useful for analyzing chemical production terms within selected grid cells, it is computationally challenging to use this approach for source attribution to specific emissions sources across the full model domain.

Evaluating the accuracy of source apportionment model results is challenging, because source contribution of secondary pollutants cannot be assessed independently based on monitoring data. Previous PM_{2.5} source apportionment implementations have been evaluated by comparing source contributions to changes in PM_{2.5} using brute force source model sensitivity simulations and by evaluating conservation of mass in the source apportionment results (Kwok et al., 2013; Z. Wang et al., 2009). Source apportionment and brute force source sensitivity methods should provide similar results when O₃ has a linear or nearly linear sensitivity to changes in precursors' emissions. Therefore, comparisons to sensitivity simulations can be useful for evaluating source apportionment methods. However, in cases where O₃ has a strong nonlinear dependence on precursors, such as the sensitivity to NO_x under radical limited conditions, source apportionment and sensitivity approaches can provide different results. For example, Emmons et al. (2012) found differences of a factor of 2–4 when comparing the MOZART O₃ source apportionment method to 20 % perturbations in pre-

Table 1. Maximum incremental reactivity in CB05 VOC species on ozone production.

CB05 VOC name	CMAQ acronym	Number of carbon atoms	MIR
Acetaldehyde	ALD2	2	4.45
Higher aldehydes	ALDX	2	6.81
Ethene	ETH	2	4.37
Ethane	ETHA	2	0.11
Ethanol	ETOH	2	1.04
Formaldehyde	FORM	1	4.50
Internal olefin	IOLE	4	13.11
Isoprene	ISOP	5	11.56
Methanol	MEOH	1	0.36
Olefin	OLE	2	8.24
Paraffin	PAR	1	0.32
Monoterpenes	TERP	10	8.82
Toluene	TOL	7	2.94
Xylene	XYL	8	14.79

cursor NO_x emissions. Dunker et al. (2002) compared CAMx O₃ source attributions using OSAT and DDM sensitivity simulations and found that the two methods gave similar spatial distributions and that DDM sensitivity simulations explained about 70 % of the modeled O₃ concentration. Zhang et al. (2005) compared CAMx OSAT, DDM and process analysis methods and also found that each method provided generally consistent assessments of source contributions to O₃, with the exception of urban areas in which O₃ had negative sensitivity to NO_x. In each of the studies described above, small emissions reductions or first-order DDM sensitivities do not account for nonlinearity in the O₃ response to precursors and may not provide a reliable test for evaluating source apportionment approaches. Tonnesen (1999) found that model sensitivity analyses using small emissions changes did not accurately characterize the effect of uncertainty in model inputs on O₃ attainment strategies and recommended that large emissions changes should be used to assess model sensitivity. Therefore, similar to previous studies, ISAM O₃ contributions are compared here with model sensitivity simulations to determine if ISAM provides generally consistent results. However, instead of using small emissions changes, we use brute force zero-out scenarios of emissions sectors to account more reliably for nonlinearity in the O₃ response to changes in precursors. While we expect that there will be some differences in the sensitivity and source apportionment results, especially for strongly nonlinear NO_x sensitivity in urban areas, we believe this approach to be useful for evaluating the accuracy of ISAM O₃ source attributions for conditions that do not have strongly nonlinear sensitivities.

Table 2. All-hour domain averaged NO_x and VOC emissions rates for Californian 12 km domain during the period 28 June–5 July 2007.

Emission sectors	NO _x emis. mole s ⁻¹	% of total NO _x emis.	VOC emis. moleC s ⁻¹	% of total VOC emis.	VOC / NO _x moleC mole ⁻¹
BEIS (BIOG)	76.3	9.1	20939.2	88.9	274.4
Marine (MARINE)	28.7	3.4	7.5	0.0	0.3
Fire (FIRE)	10.7	1.3	312.7	1.3	29.2
Non-road (NNRD)	115.4	13.7	469.7	2.0	4.1
On-road (ONRD)	413.7	49.1	535.7	2.3	1.3
Mexican point sources (MEX)	6.6	0.8	6.6	0.0	1.0
Elec. gen. units (EGU)	21	2.5	2.1	0.0	0.1
Non-elec. gen. units (Non-EGU)	36.9	4.4	25.5	0.1	0.7
Untraced emissions (OTHR)	133.1	15.8	1264.9	5.4	9.5
Emission totals	842.4		23 563.9		28.0

3 Method

3.1 Implementation overview

The ISAM for O₃ has been implemented in the CMAQ version 5.0.2 model, which was developed by the United States Environmental Protection Agency (EPA) and is used by EPA, other regulatory agencies, and academic institutions to characterize local to continental-scale ozone formation and transport (Byun and Schere, 2006; Foley et al., 2010). The ISAM O₃ source apportionment implementation is designed to track the contribution from user selected categories of NO_x and VOC emissions to model estimated NO_x, VOCs, and ozone concentration and deposition. In addition to precursor emissions, the model tracks O₃, NO_x, and VOCs from the lateral boundary conditions, and initial conditions. Precursor emissions tracers can be defined geographically using an additional model input file that assigns the fractional area of each model grid cell to specified subregions (typically a state or province). Precursor emissions tracers can also be defined by source sector (typically, major point sources, mobile sources, biogenic sources, etc.) or for specific point sources with a tag identification environment variable associated with each point source stack in the model ready input file. The user may also combine the emissions source sector and the specific geographic subregion functionality. This implementation adds to the previous version of PM_{2.5} ISAM code and uses many of the same approaches that were presented in detail by Kwok et al. (2013). Only new ozone specific physical and chemical algorithms are described here.

The ozone source apportionment approach implemented in CMAQ is similar to the approach implemented in CAMx (ENVIRON, 2013), but uses tracers for individual nitrogen and VOC species, whereas CAMx uses two tracers to represent the families of NO_x and VOCs. Ozone production is attributed to either VOC or NO_x emissions sources based on the ozone chemical formation regime that is estimated using the PH₂O₂ / PHNO₃ indicator ratio, similar to the implementation in CAMx. As described above, the bulk concentration of each VOC and NO_x species is equal to the sum of the tracers used to identify the sources of VOCs and NO_x. The bulk O₃ concentration in each model grid cell is equal to the sum of O₃ tracers that were produced in either VOC- or NO_x-sensitive conditions:

$$O_{3\text{bulk}} = \sum_{\text{tag}} O_3 V_{\text{tag}} + \sum_{\text{tag}} O_3 N_{\text{tag}}, \quad (15)$$

where $O_3 V_{\text{tag}}$ and $O_3 N_{\text{tag}}$ are the VOC-sensitive and NO_x-sensitive O₃ attributed to each tag source, respectively. The implementation described here is for the Carbon Bond 2005 (CB05) photochemical mechanism that uses a reduced set of model VOC species (Yarwood et al., 2005). Tracers are defined for the 14 CB05 VOC species contributing to ozone formation including acetaldehyde (ALD2), higher aldehydes (ALDX), ethene (ETH), ethane (ETHA), ethanol (ETOH), formaldehyde (FORM), internal olefin (IOLE), isoprene (ISOP), methanol (MEOH), olefin (OLE), paraffin (PAR), monoterpene (TERP), toluene (TOL), and xylene (XYL) (Table 1). The nine nitrogen compounds in CB05 that participate in the O₃ formation chemistry include NO, NO₂, nitrogen

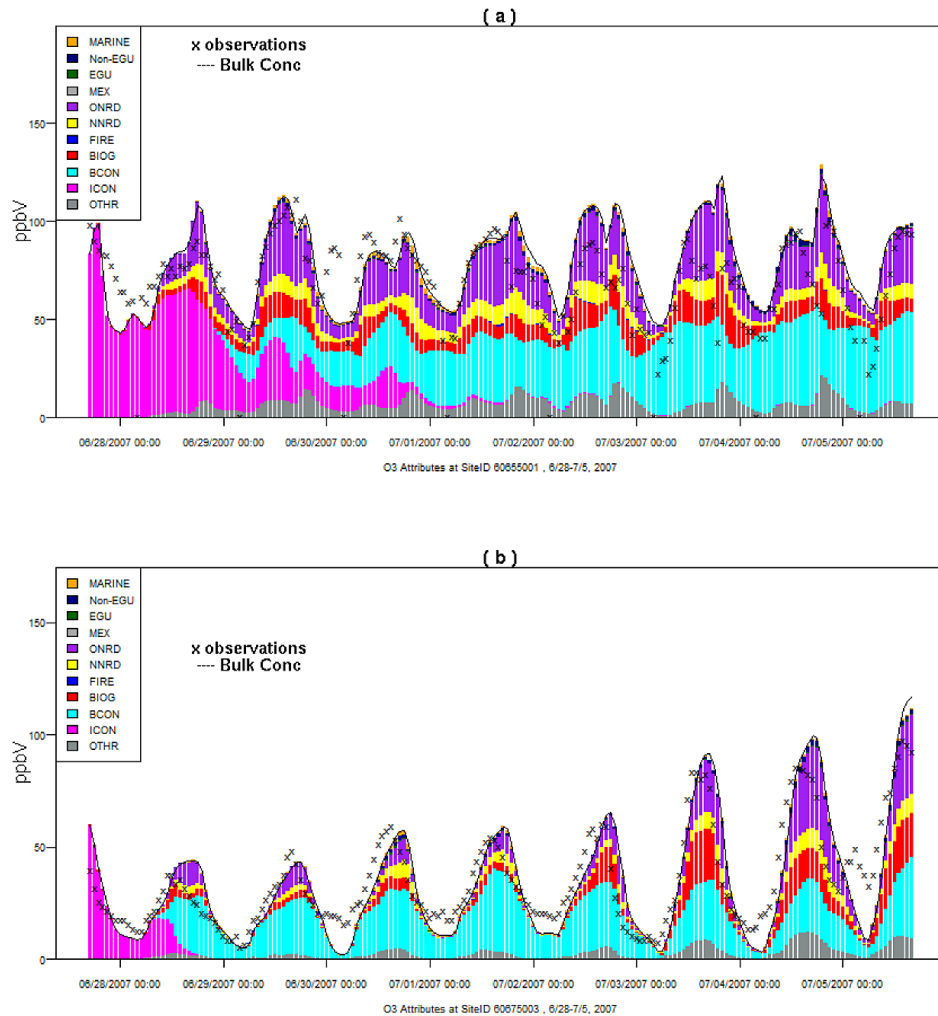


Figure 1. Hourly time series of O₃ observations (crosses) at sites of the California Air Resources Board monitoring network; and the corresponding CMAQ-ISAM sector breakdowns (stacking colored bars). Locations are (a) Riverside and (b) Sacramento. The colors represent sector sources: marine (MARINE, orange), non-electricity generation units (Non-EGU, deep blue), electricity generation units (EGU, green), other point sources (MEX, light grey), on-road mobile (ONRD, purple), non-road mobile (NNRD, yellow), wildfires (FIRE, blue), biogenic (BIOG, red), boundary conditions (BCON, cyan), initial conditions (ICON, magenta), and remaining unspecified emissions (OTHR, grey). The solid black trace on top of the bars denotes the modeled bulk O₃ concentration.

trioxide (NO₃), dinitrogen pentoxide (N₂O₅), nitrous acid (HONO), peroxyacyl nitrates (PAN), higher peroxyacyl nitrates (PANX), peroxyntic acid (PNA), and organic nitrates (NTR).

ISAM apportions CMAQ-calculated wet and dry deposition of O₃, NO_x, and all VOC species into individual sources as done in the previous PM_{2.5} ISAM code. Both of these processes follow simple linear algorithms where the mass removed is a function of existing mass and a removal coefficient and thus did not require additional consideration for the ozone implementation.

In the CMAQ gas phase chemistry module, nitrogen species are updated by chemical sensitivity approach as in Kwok et al. (2013). Likewise, the explicit VOC tracers are

entered into the same algorithm in a matrix solution:

$$[\text{VOC}_{s,\text{tag}}^{\text{new}}] = \left(\mathbf{I} - \frac{\Delta t}{2} \mathbf{J} \right)^{-1} \left(\mathbf{I} + \frac{\Delta t}{2} \mathbf{J} \right) [\text{VOC}_{s,\text{tag}}^{\text{old}}], \quad (16)$$

where $\text{VOC}_{s,\text{tag}}^{\text{new/old}}$ is the VOC species s for sector tag before (old) or after (new) the Jacobian calculation; \mathbf{I} the identity matrix; \mathbf{J} the Jacobian matrix calculated based on the average of bulk concentrations before and after any gas-phase solver for CB05 model species ($\frac{[C_{S,\text{bulk}}^{\text{new}}] + [C_{S,\text{bulk}}^{\text{old}}]}{2}$) (e.g., Euler backward method, which is used here). This system is solved by decomposing $(\mathbf{I} - \frac{\Delta t}{2} \mathbf{J})^{-1} (\mathbf{I} + \frac{\Delta t}{2} \mathbf{J})$ into a product of lower and upper triangular matrices, which is known as LU decomposition. The solution is obtained only once for every model

synchronization time step Δt instead of incremental chemical time steps to increase computational efficiency at little expense to accuracy as was previously shown in the original implementation of the CMAQ DDM (Hakami, 2004).

3.2 Ozone regime indicators

The ratio of the instantaneous production rates of hydrogen peroxide to nitric acid ($\text{PH}_2\text{O}_2 / \text{PHNO}_3$) is used as an indicator to distinguish photochemical regimes, in which PO_3 is primarily sensitive to either VOCs or NO_x . Kleinman et al. (1994) evaluated the dependence of H_2O_2 on high and low NO_x photochemical regimes and Sillman (1995) proposed that a ratio of $\text{H}_2\text{O}_2 / \text{HNO}_3$ equal to 0.35 should distinguish NO_x -sensitive regimes ($\text{H}_2\text{O}_2 / \text{HNO}_3 > 0.35$) versus VOC-sensitive regimes ($\text{H}_2\text{O}_2 / \text{HNO}_3 < 0.35$). Sillman (1995) evaluated the modeled daily maximum O_3 sensitivity to VOCs and NO_x as a function of the $\text{H}_2\text{O}_2 / \text{HNO}_3$ ratio and found that transition from VOC-sensitive to NO_x -sensitive regimes occurred at ratios in the range of 0.35–0.6, with the higher ratio occurring in aged air masses, in which concentrations of H_2O_2 and HNO_3 may have been affected by deposition. Tonnesen and Dennis (2000a, b) evaluated indicators of instantaneous production of O_x (PO_x) and of daily maximum O_3 concentration and found that indicator ratios had mixed performance for daily maximum O_3 concentration because of the effects of background concentrations and deposition. However, Tonnesen and Dennis (2000a) found that $\text{PH}_2\text{O}_2 / \text{PHNO}_3$ was an extremely robust indicator for instantaneous PO_x sensitivity. Numerous other studies have evaluated the performance of several different indicator ratios for daily maximum O_3 sensitivity to VOCs and NO_x (Milford et al., 1994; Lu and Chang, 1998; Vogel et al., 1999; Sillman et al., 2000; Andreani-Aksoyoglu, 2002; Jimenez and Baldasano, 2004; Liang et al., 2006; Y. Zhang et al., 2009; Peng et al., 2011; Torres-Jordan et al., 2012). While these studies have found variable and sometimes conflicting results for the usefulness of indicator ratios, each evaluated indicators of daily maximum O_3 concentration rather than PO_3 . Based on the most commonly used indicator ratio $\text{PH}_2\text{O}_2 / \text{PHNO}_3$, ISAM attributes the instantaneous production term PO_3 to either VOC or NO_x tracers.

Because O_3 production and loss processes occur simultaneously, the total PO_3 and DO_3 terms are calculated and used to update the O_3 tracers at each time step in the numerical chemistry solver used in the model, using the same approach as CAMx (ENVIRON, 2013). When PO_3 occurs in any grid cell, $\text{PH}_2\text{O}_2 / \text{PHNO}_3$ is used to determine if PO_3 is primarily NO_x - or VOC-sensitive (above or below 0.35, respectively), and the O_3 tracers are updated with the production to intermediate $\text{O}_3\text{N}_{\text{tag}}^{\text{middle}}$ and $\text{O}_3\text{V}_{\text{tag}}^{\text{middle}}$ using

$$\text{O}_3\text{N}_{\text{tag}}^{\text{middle}} = \text{O}_3\text{N}_{\text{tag}}^{\text{old}} + \text{PO}_3^{\text{bulk}}$$

$$\times \frac{\text{NO}_{\text{tag}}^{\text{old}} + \text{NO}_{2\text{tag}}^{\text{old}}}{\sum_{\text{tag}} (\text{NO}_{\text{tag}}^{\text{old}} + \text{NO}_{2\text{tag}}^{\text{old}})} \text{NO}_x\text{-sensitive}, \quad (17)$$

$$\begin{aligned} \text{O}_3\text{V}_{\text{tag}}^{\text{middle}} &= \text{O}_3\text{V}_{\text{tag}}^{\text{old}} + \text{PO}_3^{\text{bulk}} \\ &\times \frac{\sum_s (\text{VOC}_{s,\text{tag}}^{\text{old}} \times \text{MIR}_s)}{\sum_s \sum_s (\text{VOC}_{s,\text{tag}}^{\text{old}} \times \text{MIR}_s)} \text{VOC-sensitive}. \quad (18) \end{aligned}$$

Here, $\text{VOC}_{s,\text{tag}}^{\text{old}}$ is the concentration of VOC species s for source sector tag. $\text{PO}_3^{\text{bulk}}$ is the production of ozone in the grid cell. Table 1 lists the maximum incremental reactivity (MIR) for each VOC species s , developed by Carter (1994) and tabulated by ENVIRON (2013), that is used to approximate the relative ozone forming potential of the VOC species. Carter (1994) also described alternative reactivity methods such as maximum ozone incremental reactivity (MOIR), and equal benefit incremental reactivity (EBIR). These alternate scales were also evaluated but did not provide significantly different results.

Following the ozone production apportionment, subsequent apportionment of ozone destruction (where $\text{DO}_3 \leq 0$) assumes only its depletion in both regimes for each sector:

$$\begin{aligned} \text{O}_3\text{X}_{\text{tag}}^{\text{new}} &= \text{O}_3\text{X}_{\text{tag}}^{\text{middle}} + \text{DO}_3^{\text{bulk}} \\ &\times \frac{\text{O}_3\text{X}_{\text{tag}}^{\text{middle}}}{\sum_{\text{tag}} (\text{O}_3\text{N}_{\text{tag}}^{\text{middle}} + \text{O}_3\text{V}_{\text{tag}}^{\text{middle}})}, \quad (19) \end{aligned}$$

where X is either N or V.

4 Application and evaluation

A model simulation from 28 June to 5 July 2007 for the State of California (CA) using 12 km sized grid cells (79 columns and 106 rows) and 24 vertical layers was used to evaluate the CMAQ ozone ISAM. Anthropogenic emissions inputs were based on the 2008 National Emission Inventory (NEI) version 2 (U.S. Environmental Protection Agency, 2013). Year specific emissions were included for electrical generating units. Meteorological inputs were generated using the Weather Research Forecasting (WRF) model (Skamarock et al., 2008). Biogenic VOC and NO_x emissions were estimated with the Biogenic Emissions Inventory System (BEIS) version 3.14 using temperature and solar radiation from the WRF model as inputs to BEIS (Carlton and Baker, 2011). Mexican emissions were projected from a 1999 inventory (U.S. Environmental Protection Agency, 2011b). The 12 km model domain was nested in a 36 km continental domain, and boundary inflow to the 36 km domain was based on spatially and temporally variant concentration data from a 2007 year-specific annual GEOS-Chem version 8-03-02 simulation (Harvard University, 2012).

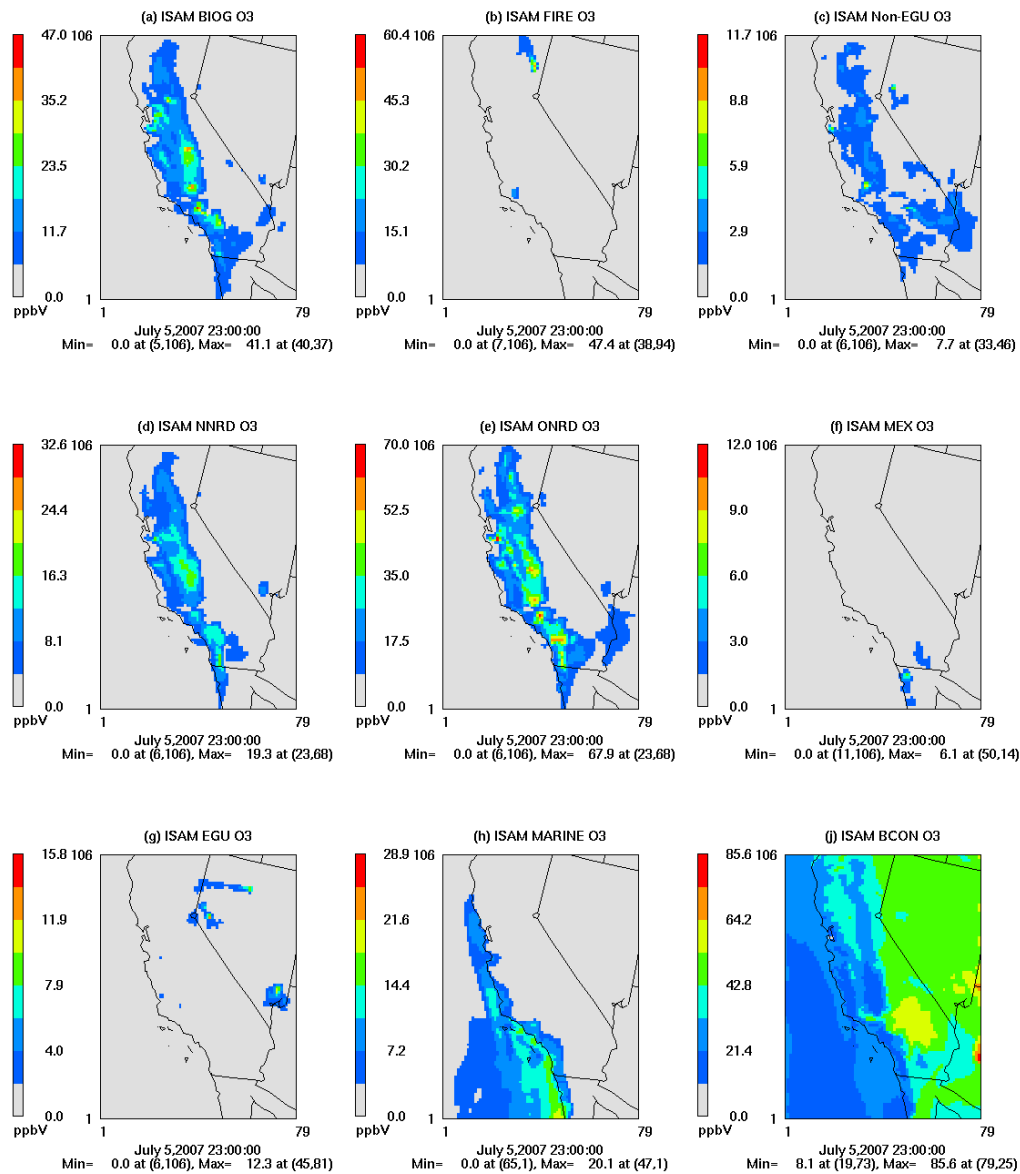


Figure 2. Spatial tiles of nine source sectors contributing to ambient O_3 , at 23:00 UTC (16:00 PDT) 5 July 2007. (a) biogenic BIOG, (b) wildfires FIRE, (c) non-electricity generation units Non-EGU, (d) non-road mobile NNRD, (e) on-road mobile ONRD, (f) Mexican point sources MEX, (g) electricity generation units EGU, (h) marine MARINE, and (j) boundary conditions BCON. Note different scales across the tiles.

To demonstrate the functionality of ISAM, eight emission sectors were chosen as tracked contributors to ozone formation. The five point source sectors represented electricity generating units (EGU), non-electricity generating units (Non-EGU), wildfires (FIRE), commercial marine (MARINE), and point sources in Mexico (MEX). The three area sources were on-road mobile (ONRD), non-road mobile (NNRD), and biogenic (BIOG). Tracers were also used for O_3 , VOCs and NO_x from the lateral boundary conditions (BCON) and initial conditions (ICON). Finally, a single additional tracer (OTHR) was used for all remaining emission categories that were not explicitly tracked. Table 2 displays emission rates

of NO_x and aggregated VOCs in those sectors. Percentages of the total emissions contributed by each sector are also listed for reference. For the modeled region, the leading NO_x emissions sectors by mass were ONRD (49.1%), NNRD (13.7%) and BIOG (9.1%), though the untracked emissions accounted for 15.8%. VOC emissions were dominated mostly by BIOG (88.9%). ISAM also has the capability to track regional sources with a user-provided map file in IOAPI/netCDF format and specific flagged point sources. Further details of the brute force setup are described in Sect. 4.2.

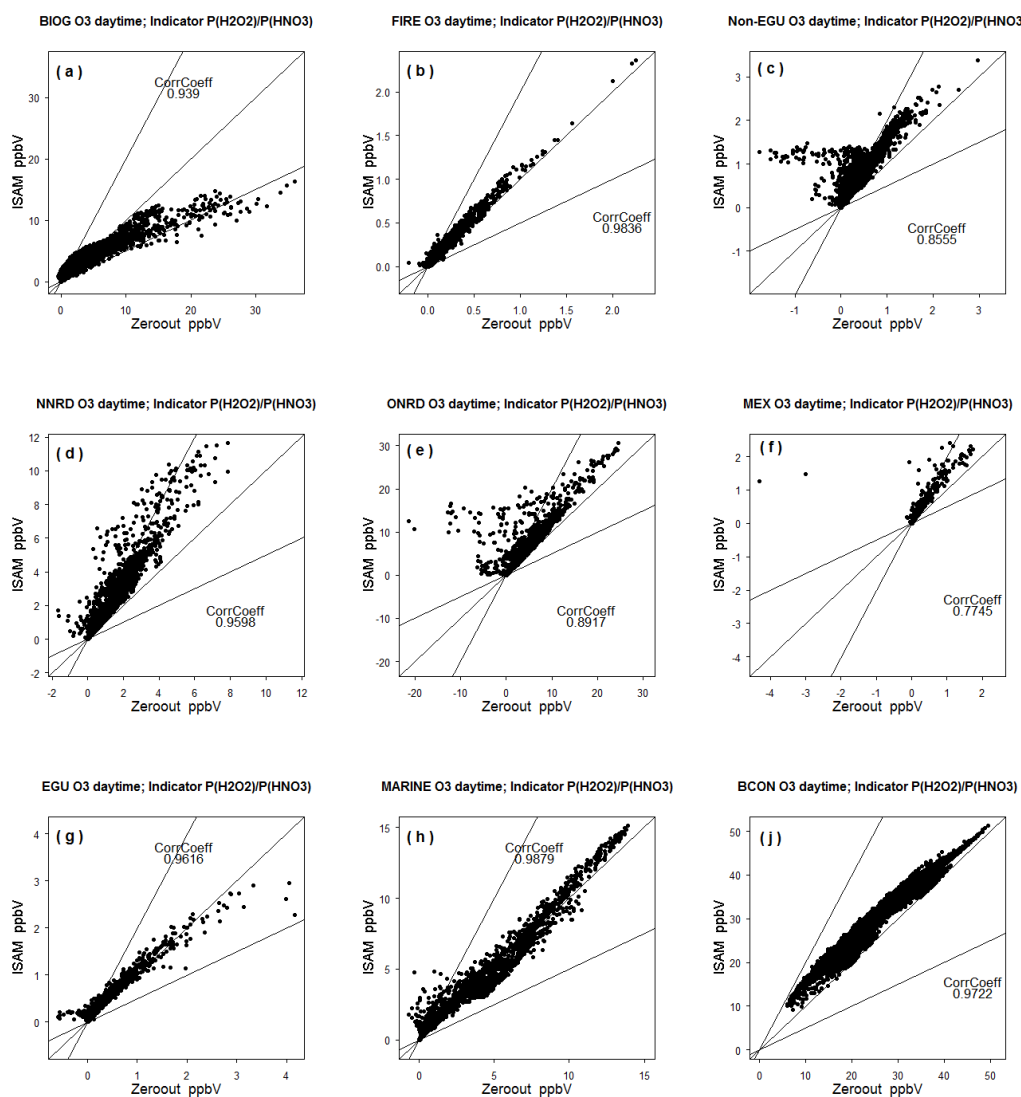


Figure 3. ISAM/both-out O₃ comparison for each sector during daytime hours. The sectors are (a) biogenic BIOG, (b) wildfires FIRE, (c) non-electricity generation units Non-EGU, (d) non-road mobile NNRD, (e) on-road mobile ONRD, (f) other point sources MEX, (g) electricity generation units EGU, (h) marine MARINE, and (j) boundary conditions BCON. Note different scales across the panels.

4.1 Sector contributions

Figure 1 displays spatial plots of individual contributing sectors to ambient O₃ in CA at 16:00LT (local time) on 5 July 2007. On this day, meteorological conditions were generally stagnant, sunny with light northerly to northwesterly winds. The CMAQ model performed well this day with an O₃ bias of 4.7 ppb (parts per billion) and average error of 9 ppb across the domain during daytime hours. For this application, the BCON contribution (Fig. 1j) is largest with contribution from 20 to 40 ppb in coastal CA and contributions of 40–60 ppb in eastern CA. Contributions from surface emissions sectors including ONRD and NNRD are also notable with contributions to O₃ as much as 64 ppb near urban areas. BIOG emissions were also an important contributor to O₃

with a maximum of 39 ppb in the central valley. The elevated point source emissions sectors of EGU, Non-EGU, MEX, and MARINE contribute relatively less to O₃ at the surface layer. Spatial correspondence is evident among O₃ (Fig. 1), NO_x, and VOC concentrations (Supplement Figs. S1, S2), as well as NO_x and VOC emissions (Figs. S3, S4) for most sectors suggesting that ISAM is predicting realistic source signatures. For example, the wildfire in northern CA is reflected in O₃ (Fig. 1b), precursor concentrations (Figs. S1b, S2b) and emissions (Figs. S3b, S4b). O₃ produced from emissions in the marine sector is distributed mostly along the coast (Fig. 1h), which is also seen in NO_x and VOC concentrations (Figs. S1h, S2h). The corresponding marine emission plot tiles (Figs. S3h, S4h) indicate sources mostly near the San Francisco Bay area and the Port of Los Angeles. BCON

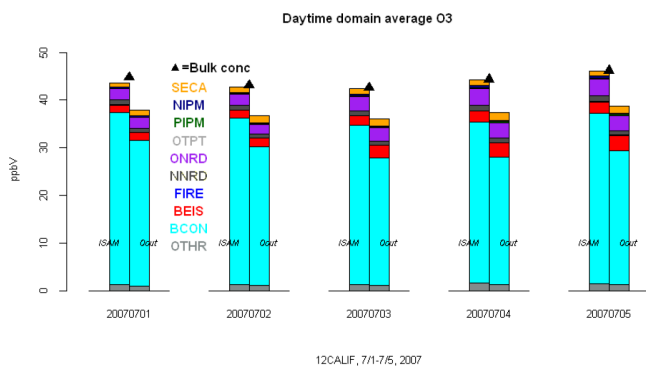


Figure 4. Daytime domain-averaged ambient O_3 , 1–5 July 2007 (28–30 June excluded due to large initial conditions influence). In the bar plot, each day consists of two stacked columns (ISAM on the left; both-out total on the right) and above them a black triangle designating bulk ambient concentration calculated from regular CMAQ. The colors represent sector sources: marine (MARINE, orange), non-electricity generation units (Non-EGU, deep blue), electricity generation units (EGU, green), other point sources (MEX, light grey), on-road mobile (ONRD, purple), non-road mobile (NNRD, yellow), wildfires (FIRE, blue), biogenic (BIOG, red), boundary conditions (BCON, cyan), and remaining unspecified emissions (OTHR, grey).

contributions are highest at the lateral edges of the domain and in areas of elevated terrain as expected.

The ISAM contributions also realistically change in time similar to bulk modeled estimates and ambient measurements. This is demonstrated for two O_3 monitor locations, at Riverside in Fig. 2a and Sacramento in Fig. 2b, where monitor data are displayed with the model simulated ozone and ISAM-attributed data. Each location had data availability at six separate monitoring sites and Fig. 2 shows the average measured and modeled quantities. Individual monitor results are shown in Fig. S5. Despite clear differences in the ozone formation behavior at the two locations, including lower O_3 concentrations and greater nighttime titration of O_3 by NO_x at the Sacramento monitor, the observed O_3 levels at the two sites are reproduced by CMAQ. Results presented in Supplement Fig. S5 and Fig. 2 demonstrate the base model's ability to capture the temporal and regional variability in observed ozone.

4.2 ISAM/brute force comparisons

The brute force or zero-out approach was used to provide an estimate of source contribution for comparison with source contribution estimated with the O_3 source apportionment algorithm. The brute force source sensitivity approach determines O_3 response to partial or total removal of an emission sector/region/species of interest, whereas ISAM was used to provide an alternate estimate of the source sector/region/species contribution to O_3 . These approaches provide similar results in linear systems and less similar results

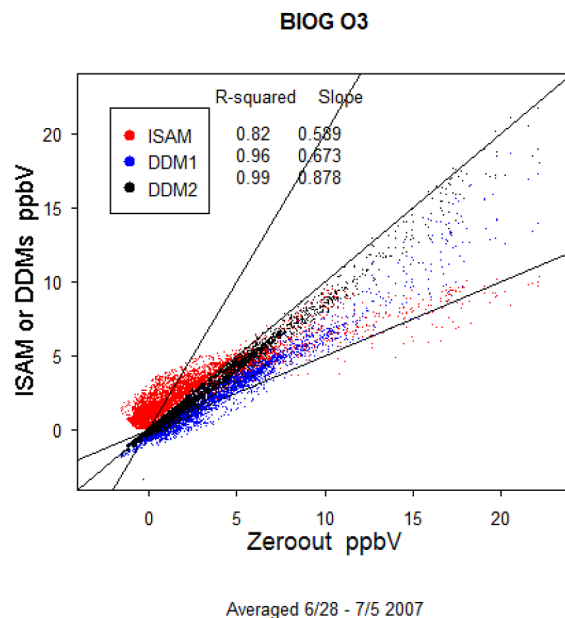


Figure 5. Scatter plots of biogenic O_3 with respect to the zero-out brute force, sampled on all-hour-averaged data. Red: ISAM, blue: first-order decoupled direct method (DDM1), black: second-order decoupled direct method (DDM2). The corresponding R squared values and regression slopes are also displayed.

in more nonlinear systems. Therefore, given the nature of these approaches, source estimates will be similar but should never match given the inherent differences in methodology. Throughout this study, three types of brute force emission data sets were constructed for each sector. The first type removes both NO_x and VOC emissions from each tracked source, denoted “both-out”. The second one only removes NO_x , denoted “N-out”. The third only removes VOCs, denoted “V-out”. Since the formation regime of boundary inflow O_3 is unknown, the both-out includes zero-out of BCON O_3 , NO , NO_2 , and the VOCs. The both-out brute force simulations were used to compare ISAM O_3 collectively from both VOC- and NO_x -sensitive regimes. The N-out was used to compare ISAM NO_x -limited O_3 (O_3N) as well as ISAM NO_x , while the V-out assessed ISAM VOC-limited O_3 (O_3V) as well as ISAM VOCs. Bearing in mind that any zero-out run is subtracted from the base case run so that the resulting difference is compared with the corresponding ISAM sector, the remainder of this manuscript will refer to this difference simply as both-out, N-out or V-out.

4.2.1 Ozone

Figure 3 compares ISAM and both-out results for O_3 from each tracked sector. Data points are daytime-averaged (06:00–18:00 Pacific daylight time, PDT) for each grid cell. In general, surface emissions such as BIOG, NNRD and ONRD (Table 2) give rise to higher surface O_3 concentra-

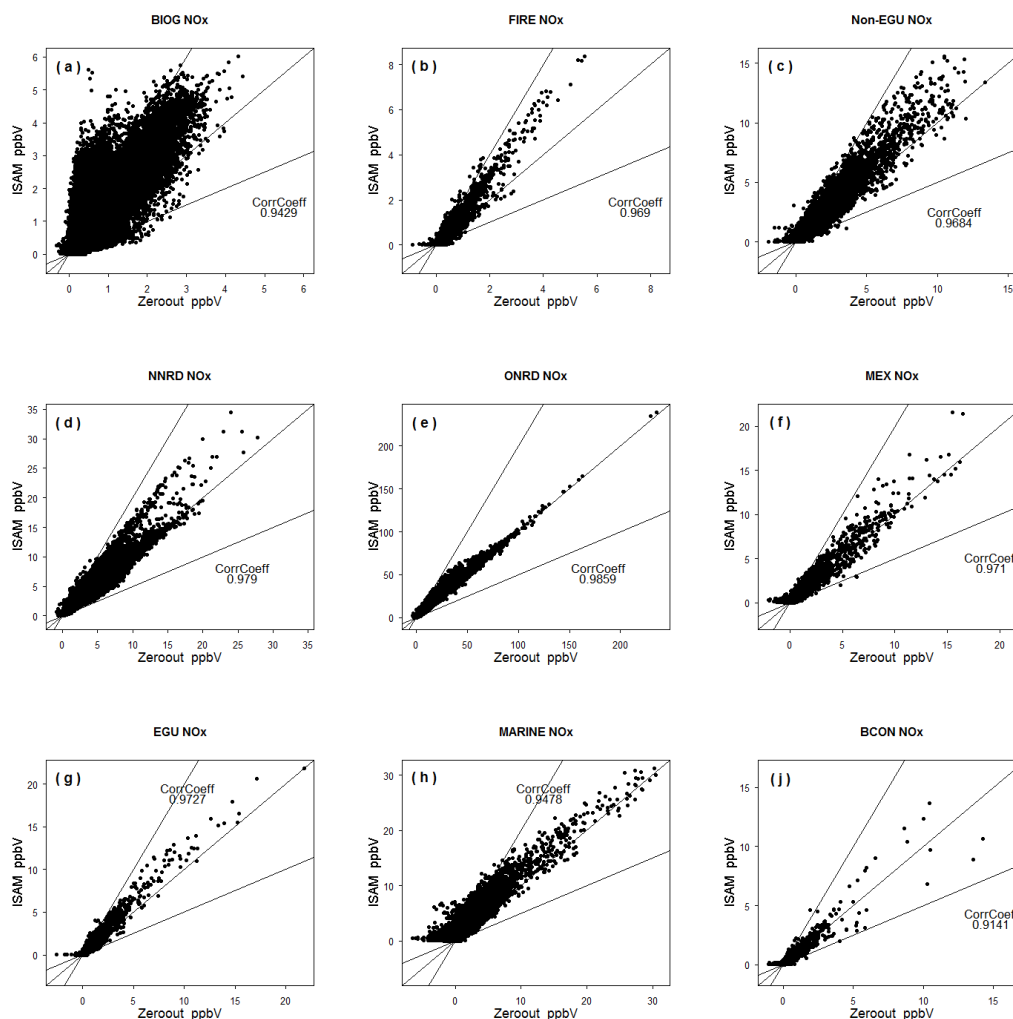


Figure 6. ISAM/N-out NO_x ($\text{NO} + \text{NO}_2$) comparison for each sector and all simulated hours. The sectors are (a) biogenic BIOG, (b) wildfires FIRE, (c) non-electricity generation units Non-EGU, (d) non-road mobile NNRD, (e) on-road mobile ONRD, (f) other point sources MEX, (g) electricity generation units EGU, (h) marine MARINE, and (j) boundary conditions BCON. Note different scales across the panels.

tions attributed to these sectors. Negative O_3 brute force response in Non-EGU, ONRD, and MEX (Figs. 3c, e, f) implies a disbenefit (i.e., O_3 increase) from removing both NO_x and VOC emissions from these sectors. This is consistent with previous model sensitivity studies which show disbenefits for NO_x emissions reductions, especially in urban areas that have typically low VOC/ NO_x ratios (Jimenez and Baldasano 2004; Zhang et al., 2009). ISAM is designed to track sources that contribute to O_3 production, and Fig. 3e shows that even in cases where O_3 has a negative sensitivity to changes in ONRD emissions in certain grid cells, those emissions in an unperturbed environment contribute to O_3 production.

The high BCON O_3 attribution by ISAM and both-out shows notable inflow of O_3 from the boundaries as shown more clearly in the stacked bar charts in Fig. 4. The global-scale GEOS-Chem model is used to provide the O_3 BC and,

therefore, source attribution of O_3 would also have to be used in GEOS-Chem to identify the sources that contribute to O_3 inflow at the boundary. However, ISAM predicts systematically more BCON O_3 than the both-out case. By comparing domain-averaged daily total O_3 of all sectors (including unspecified emissions OTHR) among ISAM, both-out and CMAQ bulk concentrations (Fig. 4), it is evident that the sum of ISAM contributions closely matches the bulk O_3 , but the sum of zero-out contributions is significantly lower than the bulk ozone concentration (15% lower on average). While ISAM appears to conserve bulk mass as designed, the zero-out case shifts the chemical system into another part of the nonlinear, often negative, O_3 response to source change. Similar qualitative features are also exhibited in total O_3 deposition (Figs. S6, S7).

Perhaps one of the most substantial ISAM/both-out comparison contrasts lies in the BIOG sector, in which ISAM

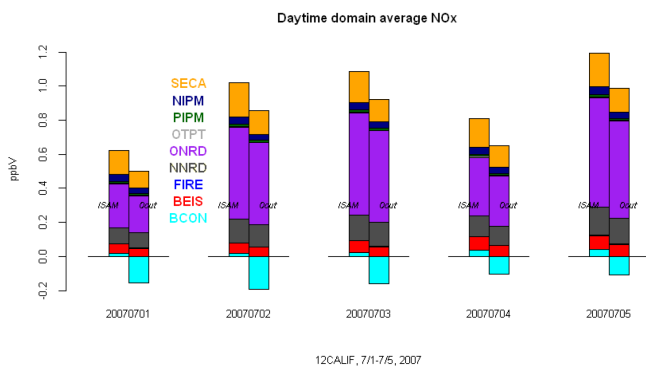


Figure 7. Daytime domain-averaged ambient NO_x ($\text{NO} + \text{NO}_2$), 1–5 July 2007 (28–30 June excluded due to large initial conditions influence). As in Fig. 4, for each day the left column designates ISAM total, and right one the zero-out. The colors represent sector sources: marine (MARINE, orange), non-electricity generation units (Non-EGU, deep blue), electricity generation units (EGU, green), other point sources (MEX, light grey), on-road mobile (ONRD, purple), non-road mobile (NNRD, yellow), wildfires (FIRE, blue), biogenic (BIOG, red), and boundary conditions (BCON, cyan).

sometimes attributes approximately half as much O_3 as both-out. Previous studies have also found strong nonlinearity in the model response to biogenic emissions (Chameides et al., 1988). Biogenic VOC emissions are generally large in rural areas with low NO_x emissions where O_3 is less sensitive to changes in VOC emissions in these areas. Yet the dominance of biogenic VOCs alone cannot adequately explain the ISAM/both-out discrepancy.

Another CMAQ diagnostic tool called decoupled direct method in three dimensions with high-order terms (HDDM-3D) (Napelenok et al., 2008) was also used to calculate the biogenic O_3 contribution. The output of CMAQ-HDDM provides both first- and second-order O_3 sensitivity to a perturbation in the biogenic sector, which is then scaled to 100 % emissions rates. With all-hour samples averaged, Fig. 5 shows that the first-order DDM approximation explains only 67 % of the brute force response, while the second-order DDM approximation explains 88 % of the zero-out response. This result suggests a highly nonlinear system in which a zero-out difference is the least likely to compare well with the source apportionment results.

4.2.2 NO_x

In addition to estimating the O_3 contribution from precursors, ISAM also allows for tracking precursor NO_x to model estimated nitrogen-containing-species concentration and deposition. Figure 6 shows ISAM/N-out NO_x scatterplots for individual sectors. For the modeled region, the most dominant sector is ONRD, followed by NNRD and MARINE, as shown more clearly in stacked bar plots in Fig. 7. Expectedly, the order in maximum NO_x concentrations in those sectors is similar to that in the domain-total NO_x emissions (Ta-

ble 2), in which ONRD and NNRD NO_x emissions dominate. It is interesting to note that the high NO_x concentrations in ONRD, NNRD and MARINE sectors are where VOC / NO_x emissions ratios are low. Conversely, the low NO_x concentration in the BIOG sector is where a very large VOC / NO_x emissions ratio occurs.

All sectors have correlation coefficients of above 0.90 for the NO_x comparison (Fig. 6). Qualitative features in total NO_x deposition (Figs. S8, S9) are also similar to those of the corresponding ambient concentrations (Figs. 6, 7).

4.2.3 VOCs

Figure 8 shows ISAM/V-out scatter plots of carbon-weighted VOCs for individual sectors, which is calculated from ISAM-output VOC species:

$$V_{\text{tag}} = \sum_s \text{VOC}_{s,\text{tag}} \times \text{NCARB}_s, \quad (20)$$

where V_{tag} is the aggregated VOC for each tag; $\text{VOC}_{s,\text{tag}}$ ISAM-output CB05 species s for each tag; and NCARB_s the number of carbon atoms in species s (see Table 1 for the complete list).

Correlations are high in most sectors except for EGU and MARINE (Fig. 8g, h), but magnitudes are also small for these two sectors. While BIOG is the most dominant VOCs sector, the high maximum VOC concentrations from FIRE do not necessarily lead to a bigger share in the domain-averaged VOC concentration (Fig. 9). In fact, domain-wide major VOC sectors are BIOG, BCON and ONRD (Fig. 9). Similar features are evident in the total VOC deposition (Figs. S10, S11).

To more closely examine the evolution of individual VOC species in the BIOG, BCON and ONRD sectors, daytime domain-averaged ambient concentrations and daily total deposition of individual VOC species are displayed (Supplement Figs. S12a, c, S13a, c, S14a, c). Furthermore, we explore the influence of gas-phase degradation of those VOCs by calculating ISAM and V-out contributions from the three sectors while turning off the gas and aerosol chemistry. The corresponding VOC breakdowns were also displayed in Supplement Figs. S12b, d, S13b, d, S14b and d. Prior to gas-phase chemistry, VOC portions are very similar between ISAM and V-out in all the three sectors. Although evolution characteristics of the VOC species with photochemistry are different across these sectors, secondary formation of ALD2, ALDX, and FORM is evident in BIOG and ONRD emissions sectors where primary emissions of the aldehydes are low. These results are consistent with the modeled VOCs' degeneration into formaldehyde (or higher aldehydes) as illustrated in Reactions 4–6. However, the evolution of BCON's aldehydes is more complicated, since both imported and secondarily formed aldehydes can be equally important, none of which were explicitly distinguished by ISAM.

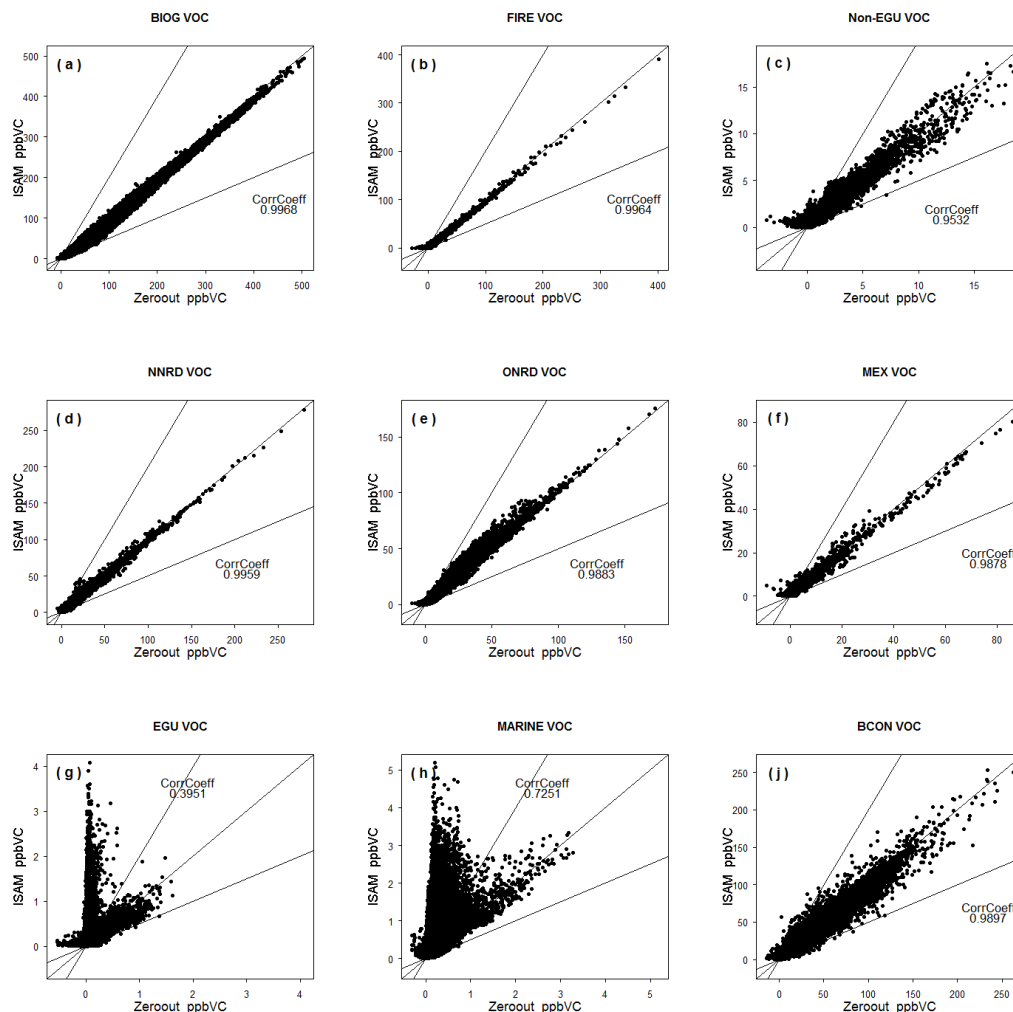


Figure 8. ISAM/V-out VOCs comparison for each sector and all simulated hours. The sectors are (a) biogenic BIOG, (b) wildfires FIRE, (c) non-electricity generation units Non-EGU, (d) non-road mobile NNRD, (e) on-road mobile ONRD, (f) other point sources MEX, (g) electricity generation units EGU, (h) marine MARINE, and (j) boundary conditions BCON. Note different scales across the panels.

5 Summary and discussion

General similarities between ISAM and zero-out cases establish credibility of the ISAM results, while specific differences, whether in magnitude or in relative portions, demonstrate different functionalities of the two approaches. The choice of appropriate methodology depends on whether source sector/region attribution or sensitivity is of interest. Implementation of O_3 tracking capability in CMAQ-ISAM for the CB05 gas-phase chemical mechanism adopts the two-regime approach, with nitrogen and VOC species explicitly tracked through all chemical transport model science processes to facilitate analysis of their chemical and physical transformations. Brute force zero-out CMAQ model simulations serve as a reference to compare the ISAM results applied for a California application in the summer of 2007. In general, correlations between ISAM/zero-out estimates

are high for both ambient concentration and deposition of O_3 for the major emissions sectors. ISAM estimates of NO_x are higher than nitrogen-out in most sectors except boundary condition. And ISAM VOC estimates are similar when compared to VOC-out in most sectors except EGU and MARINE. Differences between ISAM and zero-out were found in the tracking of O_3 from biogenic emissions, where the model sometimes predicts half of the contribution indicated by zero-out. In the condition of extremely low NO emissions in this sector, high nonlinearity in the gas phase chemistry, supported by the pronounced difference between DDM-based apportionment using first-order sensitivity coefficients and using first- and second-order coefficients, was found to be responsible for this discrepancy.

Explicit VOCs tracking, available in ISAM, also provides new opportunities to analyze species-specific ozone formation mechanisms (see Supplemental Figures). This approach

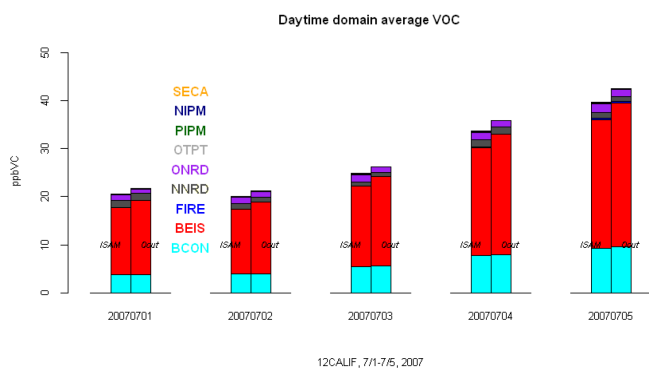


Figure 9. Daytime domain-averaged ambient VOCs, 1–5 July 2007 (28–30 June excluded due to large initial conditions influence). As in Fig. 4, for each day the left column designates ISAM total, and the right column the zero-out. The colors represent sector sources: marine (MARINE, orange), non-electricity generation units (Non-EGU, deep blue), electricity generation units (EGU, green), other point sources (MEX, light grey), on-road mobile (ONRD, purple), non-road mobile (NNRD, yellow), wildfires (FIRE, blue), biogenic (BIOG, red), and boundary conditions (BCON, cyan).

not only complements results derived from receptor-based models such as CMB and PMF, but also offers a diagnostic tool to track the chemical evolution of the VOC species that cannot be otherwise adequately explained by receptor-based models alone. In addition to providing VOC contribution information similar to a receptor-based source apportionment model, this source-based approach also estimates contribution for nitrogen species, O_3 , and deposition of each.

The source apportionment technique is recommended when an assessment of contributing sources is desired for model predicted species. Where the change in air quality resulting from perturbing contributing sources is desired, a source sensitivity approach such as brute-force or DDM may be more appropriate. Furthermore, source apportionment should generally be applied for sources or source groups that are well characterized since limitations in the emissions inventory will manifest in photochemical model and source contribution estimates.

Code availability

The implementation of the ISAM source apportionment technique for O_3 and its precursors in the CMAQ photochemical grid model presented here is freely available online at <https://www.emascenter.org>. This includes code, documentation, and a small test case for benchmarking and illustrating ISAM setup and capability.

The Supplement related to this article is available online at doi:10.5194/gmd-8-99-2015-supplement.

Acknowledgements. The authors would like to recognize the contribution of David Wong, Lara Reynolds, Allan Beidler, James Beidler, Chris Allen, and Heather Simon.

Disclaimer. Although this work was reviewed by EPA and approved for publication, it may not necessarily reflect official agency policy.

Edited by: F. O'Connor

References

- Andreani-Aksoyoglu, S., Keller, J., and Prevot, A.: Air Pollution Modelling and Simulation, Proceedings, Applicability of indicator-based approach to assess ozone sensitivities: A model study in Switzerland. Springer-Verlag Berlin, Berlin. 21–29, 2002.
- Anenberg, S. C., Horowitz, L. W., Tong, D. Q., and West, J. J.: An Estimate of the Global Burden of Anthropogenic Ozone and Fine Particulate Matter on Premature Human Mortality Using Atmospheric Modeling, *Environ. Health Perspect.*, 118, 1189–1195, 2010.
- Arunachalam, S.: Peer Review of Source Apportionment Tools in CAMx and CMAQ, UNC-Chapel Hill, Contract no. EP-D-07-102, Assignment no. 2-06, Version 2, 2010.
- Bell, M. L., McDermott, A., Zeger, S. L., Samet, J. M., and Dominici, F.: Ozone and short-term mortality in 95 US urban communities, 1987–2000, *J. Am. Med. Assoc.*, 292, 2372–2378, 2004.
- Bergin, M. S., Russell, A. G., Odman, M. T., Cohan, D. S., and Chameides, W. L.: Single-Source Impact Analysis Using Three-Dimensional Air Quality Models, *J. Air Waste Manage. Assoc.*, 58, 1351–1359, 2008.
- Buzcu, B. and Fraser, M. P.: Source identification and apportionment of volatile organic compounds in Houston, TX, *Atmos. Environ.*, 40, 2385–2400, 2006.
- Byun, D. and Schere, K. L.: Review of the governing equations, computational algorithms, and other components of the models-3 Community Multiscale Air Quality (CMAQ) modeling system, *Appl. Mech. Rev.*, 59, 51–77, 2006.
- Carlton, A. G. and Baker, K. R.: Photochemical modeling of the Ozark isoprene volcano: MEGAN, BEIS, and their impacts on air quality predictions, *Environ. Sci. Technol.*, 45, 4438–4445, 2011.
- Carter, W. P. L.: Development of ozone reactivity scales for volatile organic compounds, *J. Air Waste Manage. Assoc.*, 44, 881–899, 1994.
- Chameides, W. L., Lindsay, R. W., Richardson, J., and Kiang, C. S.: The role of biogenic hydrocarbons in urban photochemical smog – Atlanta as a case-study, *Science*, 241, 1473–1475, 1988.
- Chung, J., Wadden, R. A., and Scheff, P. A.: Development of ozone-precursor relationships using VOC receptor modeling, *Atmos. Environ.*, 30, 3167–3179, 1996.
- Cohan, D. S. and Napelenok, S. L.: Air Quality Response Modeling for Decision Support, *Atmosphere*, 2, 407–425, 2011.
- Dunker, A. M., Yarwood, G., Ortman, J. P., and Wilson, G. M.: Comparison of source apportionment and source sensitivity of

- ozone in a three-dimensional air quality model, *Environ. Sci. Technol.*, 36, 2953–2964, 2002.
- Emmons, L. K., Hess, P. G., Lamarque, J.-F., and Pfister, G. G.: Tagged ozone mechanism for MOZART-4, CAM-chem and other chemical transport models, *Geosci. Model Dev.*, 5, 1531–1542, doi:10.5194/gmd-5-1531-2012, 2012.
- ENVIRON: User's Guide Comprehensive Air Quality Model with Extensions, ENVIRON International Corporation, Novato, California, available at: www.camx.com (last access: 20 January 2015), 2013.
- Fann, N., Fulcher, C. M., and Baker, K. R.: The recent and future health burden of air pollution apportioned across 23 US sectors, *Environ. Sci. Technol.*, 47, 3580–3589, doi:10.1021/es304831q, 2013.
- Finlayson-Pitts, B. J. and Pitts Jr., J. N.: *Atmospheric Chemistry: Fundamentals and Experimental Techniques*, New York, Wiley-Interscience Publication, 1098 pp., 1986.
- Foley, K. M., Roselle, S. J., Appel, K. W., Bhawe, P. V., Pleim, J. E., Otte, T. L., Mathur, R., Sarwar, G., Young, J. O., Gilliam, R. C., Nolte, C. G., Kelly, J. T., Gilliland, A. B., and Bash, J. O.: Incremental testing of the Community Multiscale Air Quality (CMAQ) modeling system version 4.7, *Geosci. Model Dev.*, 3, 205–226, doi:10.5194/gmd-3-205-2010, 2010.
- Guinnup, D. and Collom, B.: Final Report, Vol. I: Executive Summary, OTAG Air Quality Analysis Workgroup, available at: http://capita.wustl.edu/otag/reports/aqafinvol_I/animations/v1_exsumanimb.html (last access: 20 January 2015), 1997.
- Haagen-Smit, A. J. and Fox, M. M.: Photochemical Ozone Formation with Hydrocarbons and Automobile Exhaust, *Air Repair*, 4, 105–136, doi:10.1080/00966665.1954.10467649, 1954.
- Hakami, A., Odman, M. T., and Russell, A. G.: Nonlinearity of the tropospheric ozone production, *J. Geophys. Res.*, 109, D15303, doi:10.1029/2003JD004502, 2004.
- Harvard University: GEOS-Chem Overview, available at: http://acmg.seas.harvard.edu/geos/geos_overview.html (last access: 20 January 2015), 2012.
- Henderson, B. H., Kimura, Y., McDonald-Buller, E., Allen, D. T., and Vizuete, W.: Comparison of Lagrangian Process Analysis tools for Eulerian air quality models, *Atmos. Environ.*, 45, 5200–5211, 2011.
- Husar, R. and Renard, W.: Ozone as a function of local wind direction and wind speed: Evidence of local and regional transport, available at: <http://capita.wustl.edu/otag/Reports/OTAGWIND/OTAGWIND.html> (last access: 20 January 2015), 1997.
- Jeffries, H. E. and Tonnesen, S.: A comparison of two photochemical reaction mechanisms using a mass balance and process analysis, *Atmos. Environ.*, 28, 2991–3003, 1994.
- Jimenez, P. and Baldasano, J. M.: Ozone response to precursor controls in very complex terrains: Use of photochemical indicators to assess O₃-NO_x-VOC sensitivity in the north-eastern Iberian Peninsula, *J. Geophys. Res.*, 109, D20309, doi:10.1029/2004JD004985, 2004.
- Kenski, D. M., Wadden, R. A., Scheff, P. A., and Lonneman, W. A.: Receptor Modeling Approach to VOC Emission Inventory Validation, *J. Environ. Eng.*, 121, 483–491, 1995.
- Kim, E., Brown, S. G., Hafner, H. R., and Hopke, P. K.: Characterization of non-methane volatile organic compounds sources in Houston during 2001 using positive matrix factorization, *Atmos. Environ.*, 39, 5934–5946, 2005.
- Kleinman, L., Lee, Y.-N., Springston, S. R., Nunnermacker, L., Zhou, X., Brown, R., Hallock, K., Klotz, P., Leahy, D., Lee, J. H., and Newman, L.: Ozone formation at a rural site in the south-eastern United States, *J. Geophys. Res.*, 99, 3469–3482, 1994.
- Kwok, R. H. F., Napelenok, S. L., and Baker, K. R.: Implementation and evaluation of PM_{2.5} source contribution analysis in a photochemical model, *Atmos. Environ.*, 80, 398–407, 2013.
- Langford, A. O., Aikin, K. C., Eubank, C. S., and Williams E. J.: Stratospheric contribution to high surface ozone in Colorado during springtime, *Geophys. Res. Lett.*, 36, L12801, doi:10.1029/2009GL038367, 2009.
- Lefohn, A. S., Emery, C., Shadwick, D., Wernli, H., Jung, J., and Oltmans, S. J.: Estimates of background surface ozone concentrations in the United States based on model-derived source apportionment, *Atmos. Environ.*, 84, 275–288, doi:10.1016/j.atmosenv.2013.11.033, 2014.
- Liang, J., Jackson, B., and Kaduwela, A.: Evaluation of the ability of indicator species ratios to determine the sensitivity of ozone to reductions in emissions of volatile organic compounds and oxides of nitrogen in northern California, *Atmos. Environ.*, 40, 5156–5166, 2006.
- Lin, M., Fiore, A. M., Horowitz, L. W., Cooper, O. R., Naik, V., Holloway, J., Johnson, B. J., Middlebrook, A. M., Oltmans, S. J., Pollack, I. B., Ryerson, T. B., Warner, J. X., Wiedinmyer, C., Wilson, J., and Wyman, B.: Transport of Asian ozone pollution into surface air over the western United States in spring, *J. Geophys. Res.*, 117, D00V07, doi:10.1029/2011JD016961, 2012.
- Lu, C.-H. and Chang, J.: On the indicator-based approach to assess ozone sensitivities and emission features, *J. Geophys. Res.*, 103, 3453–3462, 1998.
- Mesbah, S. M., Hakami, A., and Schott, S.: Improving NO_x Cap-and-Trade System with Adjoint-Based Emission Exchange Rates, *Environ. Sci. Technol.*, 46, 11905–11912, 2012.
- Milford, J. B., Gao, D. F., Zafirakou, A., and Pierce, T. E.: Ozone precursor levels and responses to emissions reductions – analysis of regional oxidant model results, *Atmos. Environ.*, 28, 2093–2104, 1994.
- Napelenok, S. L., Cohan, D. S., Odman, M. T., and Tonse, S.: Extension and evaluation of sensitivity analysis capabilities in a photochemical model, *Environ. Model. Softw.*, 23, 994–999, 2008.
- National Research Council: Rethinking the ozone problem in urban and regional air pollution, National Academy Press, Washington DC, 1991.
- Peng, Y.-P., Chen, K.-S., Wang, H.-K., Lai, C.-H., Lin, M.-H., and Lee, C.-H.: Applying model simulation and photochemical indicators to evaluate ozone sensitivity in southern Taiwan, *J. Environ. Sci.*, 23, 790–797, 2011.
- Pfister, G., Walters, S., Emmons, L., Edwards, D. P., and Avise, J.: Quantifying the contribution of inflow on surface ozone over California during summer 2008, *J. Geophys. Res.-Atmos.*, 118, 12282–12299, doi:10.1002/2013JD020336, 2013.
- Porter, P. S., Rao, S. T., Zurbenko, I. G., Dunker, A. M., and Wolff, G. T.: Ozone air quality over North America: Part II – An analysis of trend detection and attribution techniques, *J. Air Waste Manage. Assoc.*, 51, 283–306, 2001.
- Russell, A. and Dennis, R.: NARSTO critical review of photochemical models and modeling, *Atmos. Environ.*, 34, 2283–2324, 2000.

- Scheff, P. A. and Wadden, R. A.: Receptor Modeling of Volatile Organic-Compounds. 1. Emission Inventory and Validation, *Environ. Sci. Technol.*, 27, 617–625, 1993.
- Scheff, P. A., Wadden, R. A., Kenski, D. M., Chung, J., and Wolff, G.: Receptor model evaluation of the southeast Michigan ozone study ambient NMOC measurements, *J. Air Waste Manage. Assoc.*, 46, 1048–1057, 1996.
- Sillman, S.: The user of NO_y , H_2O_2 , and HNO_3 as indicators for ozone-NOx-hydrocarbon sensitivity in urban locations, *J. Geophys. Res.*, 100, 14175–14188, 1995.
- Sillman, S.: Ozone production efficiency and loss of NOx in power plant plumes: Photochemical model and interpretation of measurements in Tennessee, *J. Geophys. Res.-Atmos.*, 105, 9189–9202, 2000.
- Skamarock, W. C., Klemp, J. B., Dudhia, J., Gill, D. O., Barker, D. M., Duda, M. G., Huang, X. Y., Wang, W., and Powers, J. G.: A description of the advanced research WRF version 3. National Center for Atmospheric Research, Boulder, Colorado, NCAR/TN-475, 2008.
- Sudo, K. and Akimoto, H.: Global source attribution of tropospheric ozone: Long-range transport from various source regions, *J. Geophys. Res.-Atmos.*, 112, D12302 doi:10.1029/2006JD007992, 2007.
- Tonnesen, G. S.: Effects of uncertainty in the reaction of the hydroxyl radical with nitrogen dioxide on model-simulated ozone control strategies, *Atmos. Environ.*, 33, 1587–1598, 1999.
- Tonnesen, G. S. and Dennis, R. L.: Analysis of radical propagation efficiency to assess ozone sensitivity to hydrocarbons and NOx 1. Local indicators of instantaneous odd oxygen production sensitivity, *J. Geophys. Res.-Atmos.*, 105, 9213–9225, 2000a.
- Tonnesen, G. S. and Dennis, R. L.: Analysis of radical propagation efficiency to assess ozone sensitivity to hydrocarbons and NOx 2. Long-lived species as indicators of ozone concentration sensitivity, *J. Geophys. Res.-Atmos.*, 105, 9227–9241, 2000b.
- Tong, D. Q. and Mauzerall, D. L.: Summertime State-Level Source-Receptor Relationships between Nitrogen Oxides Emissions and Surface Ozone Concentrations over the Continental United States, *Environ. Sci. Technol.*, 42, 7976–7984, 2008.
- Tong, D. Q., Kang, D. W., Aneja, V. P., and Ray, J. D.: Reactive nitrogen oxides in the southeast United States national parks: source identification, origin, and process budget, *Atmos. Environ.*, 39, 315–327, 2005.
- Torres-Jardon, R., Garcia-Reynoso, J. A., Jazcilevich, A., Ruiz-Suarez, L. G., and Keener, T. C.: Assessment of the Ozone-Nitrogen Oxide-Volatile Organic Compound Sensitivity of Mexico City through an Indicator-Based Approach: Measurements and Numerical Simulations Comparison, *J. Air Waste Manage. Assoc.*, 59, 1155–1172, 2012.
- U.S. Environmental Protection Agency: Integrated Review Plan for the Ozone National Ambient Air Quality Standards Review, EPA-452/D-09-001, 2009.
- U.S. Environmental Protection Agency: North American Emissions Inventories – Mexico, available at: <http://www.epa.gov/ttnchie1/net/mexico.html>, 2011.
- U.S. Environmental Protection Agency: The National Emissions Inventory: 2008 National Emissions Inventory Data, available at: <http://www.epa.gov/ttnchie1/net/2008inventory.html> (last access: 20 January 2015), 2013.
- Vogel, B., Riemer, N., Vogel, H., and Fiedler, F.: Findings on NO_y as an indicator for ozone sensitivity based on different numerical simulations, *J. Geophys. Res.*, 104, 3605–3620, 1999.
- Wang, X., Li, J., Zhang, Y., Xie, S., and Tang, X.: Ozone source attribution during a severe photochemical smog episode in Beijing, China, *Sci. China Ser. B*, 52, 1270–1280, 2009.
- Wang, Z. S., Chien C.-J., and Tonnesen, G. S.: Development of a tagged species source apportionment algorithm to characterize three-dimensional transport and transformation of precursors and secondary pollutants, *J. Geophys. Res.*, 114, D21206, doi:10.1029/2008JD010846, 2009.
- Yarwood, G., Rao, S., Yocke, M., and Whitten, G. Z.: Updates to the carbon bond chemical mechanism: CB05, Final Report to U.S.EPA, RT-04-00675, 2005.
- Ying, Q. and Krishnan, A.: Source contributions of volatile organic compounds to ozone formation in southeast Texas, *J. Geophys. Res.-Atmos.*, 115, D17306, doi:10.1029/2010JD013931, 2010.
- Zhang, L., Jacob, D. J., Boersma, K. F., Jaffe, D. A., Olson, J. R., Bowman, K. W., Worden, J. R., Thompson, A. M., Avery, M. A., Cohen, R. C., Dibb, J. E., Flock, F. M., Fuelberg, H. E., Huey, L. G., McMillan, W. W., Singh, H. B., and Weinheimer, A. J.: Transpacific transport of ozone pollution and the effect of recent Asian emission increases on air quality in North America: an integrated analysis using satellite, aircraft, ozonesonde, and surface observations, *Atmos. Chem. Phys.*, 8, 6117–6136, doi:10.5194/acp-8-6117-2008, 2008.
- Zhang, L., Jacob, D. J., Kopacz, M., Henze, D. K., Singh, K., and Jaffe, D. A.: Intercontinental source attribution of ozone pollution at western US sites using an adjoint method, *Geophys. Res. Lett.*, 36, L11810, doi:10.1029/2009GL037950, 2009.
- Zhang, Y., Vijayaraghavan, K., and Seigneur, C.: Evaluation of three probing techniques in a three-dimensional air quality model, *J. Geophys. Res.-Atmos.*, 110, D02305, doi:10.1029/2004JD005248, 2005.
- Zhang, Y., Wen, X.-Y., Wang, K., Vijayaraghavan, K., and Jacobson, M. Z.: Probing into regional O_3 and particulate matter in the United States: 2. An examination of formation mechanisms through a process analysis technique and sensitivity study, *J. Geophys. Res.*, 114, D22305, doi:10.1029/2009JD011900, 2009.